Chalcogenide Letters Vol. 12, No. 7, July 2015, p. 339 - 347

SYNTHESIS, SPECTROSCOPIC INVESTIGATION, AND MOLECULAR INTERACTIONS BETWEEN ACIVICIN AND CdSe QUANTUM DOTS

S.E. ALGARNI[a*], S.R. ALHARBI[a], M.S. ABD EL SADEK[b],
H.S. EL-SHESHTAWY[c]
[a]*Physics Department, Science Faculty for Girls, King Abdulaziz University, Jeddah- Saudi Arabia*
[b]*Nanomaterials Lab., Physics Department, Faculty of Science, South Valley University, Qena- Egypt.*
[c]*Biotechnology and Fish Processing Department, Faculty of Aquatic and Fisheries Sciences, Kafrelsheikh University, Kafrelsheikh-Egypt*

Water-Soluble and fluorescent thiol capped CdSe quantum dots (QDs) were synthesized by chemical rout. The structure of CdSe QDs was investigated by means of X–ray diffraction (XRD), energy–dispersive X–ray analysis (EDX), UV–visible, Fourier transform infrared (FT–IR) spectroscopy and transmission electron microscopy (TEM). The crystal phase of the CdSe QDs confirmed with XRD diffraction technique. The average size of CdSe QDs was calculated to be 3 nm by different spectroscopic techniques. CdSe capped with mercaptopropionic acid (MPA) shows a characteristic fluorescent peak at 590 nm, which is highly dependant on the pH value. The interaction of the water-soluble MPA–CdSe and acivicin (AC) was investigated in 50 mM sodium acetate buffer pH 7.4 by fluorescence spectroscopy. The interaction between acivicin and MPA–CdSe shows a dynamic quenching process. Analysis of the circular dichorism (CD) spectra indicated higher interaction of the MPA–CdSe-AC complex with human serum albumin than the individual AC drug.

(Received April 5, 2015; Acepted July 1, 2015)

Keywords: CdSe QDs, Antibiotics Interactions, Acivicin, Optical Properties, Quenching Mechanisms.

1. Introduction

Recently, quantum dots (QDs), the nanocrystals with a size range from 10-100 nm, attract the attention of researchers particularly, in biological imaging and biomolecular applications [1-6]. The exceptional photophysical properties such as broad absorption spectra, narrow and symmetric emission spectra, and the ability to tune such features were the potential for biomedical applications [7, 8]. However, the concern related to the health risks of QDs still under debate. QDs toxicity reported to largely depend on the physicochemical properties such as, size, charge, and concentration, in addition to the environmental conditions. QDs dosage/exposure concentration is a vital condition for the cytotexcocity, for example, 10-fold higher concentration of $CdCl_2$ (20 μM) was required to induce equivalent mortality as a solution of 2 μM QDs [9], on the other hand, ZnS capped CdSe QDs was not harmful to Sprague–Dawley rats in both short and long–term [10]. Hence, the lethal dose [11] and the intracellular QDs concentration not the extracellular are important factors in QDs cytotoxicity both *in vivo* and *in vitro* investigation [12].

Recently, antibiotic resistance bacteria such as *Staphylococcus aureus*, *methicillin-resistant S. aureus* (MRSA) have become a serious problem for public health [13]. Different pathways for antibiotic resistance mechanism have been reported [14]. Particularly, both the degradation and the leakage of the antibiotics outside the cell decrease the binding and

* Corresponding author: algarnisabah@gmail.com

significantly loose the activity. One of the promising approaches to overcome the problem is to use the antibiotic-nanoparticles bioconjugate to ensure strong binding and high activity towards the target cells. This approach is based on enhancing the activity of the antibiotics by their attachments to the nanoparticles [15].

Herein, we are investigating the *in vitro* interaction between MPA–CdSe nanocrystal and acivicin antibiotic molecule (Fig.1). Acivicin, (αS,5S)- α-amino-3-chloro-4,5-dihydro-5-isoxazoleacetic acid, is a potent antitumor antibiotic, and show antifungal activity [16]. Different spectroscopic techniques such as fluorescence spectra, absorption spectra, and circular dichroism were used to study the molecular and mechanism interaction.

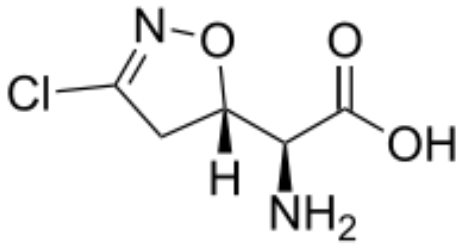

Fig. 1. Acivicin Structure

2. Material and Methods

All the chemicals used in this work were of analytical grade or the highest purity available and obtained from commercial sources and used without further purification. $CdCl_2.2.5H_2O$, acivicin were purchased from Sigma-Aldrich (Germany). Powder X–ray diffraction (XRD) analysis was carried out with X–ray diffractometer, D8 ADVANCE type (BRUKER–AXS Germany) with CuK_α (/ = 0.15406 nm) radiation. Morphology and structural of the synthesized materials were investigated by transmission electron microscopy (TEM, JEOL JEM-1230 with accelerating voltage of 120 kV) with EDX detector unit attached to the system. FT–IR spectra were recorded with a JASCO FT–IR spectrometer within the range of 500 – 4000 cm^{-1}. Room temperature UV–Visible absorption spectra were measured using a JASCO V-760 UV–VIS–NIR spectrophotometer. Photoluminescence measurements were performed at room temperature using JASCO FP-8500 fluorescence spectrofluorometer (excitation wavelength λ_{exc} was set at 390 nm). Circular Dichroism spectra measurements were performed on JASCO Circular Dichroism Spectrometer.

2.1 Synthesis of CdSe Quantum Dots

CdSe was prepared according to literature procedures with modification [17]. The alkaline selenium aqueous solution was prepared as follows: 0.56 mol of NaOH and 0.0025 mol of elemental Se were added to 50 ml of distilled water. The temperature of the mixture reached about 80°C due to the exothermic dissolution of NaOH, which guarantee the dissolution of elemental Se. Then, $CdCl_2.2.5H_2O$ (0.0026 mol) was added to 10 ml of MPA aqueous solution (0.3M) and the mixture was added to the alkaline selenium aqueous solution under continuous stirring. A red-brown precipitate of CdSe capped with MPA is evolved. After being filtered and washed with dilute HCl solution (0.1M) and distilled water, the precipitate was dried under vacuum at 50°C for 4 h. The final product was collected for characterization.

3. Results and Discussion

3.1. Structural and Morphology of MPA–CdSe Nanocrystals

The MPA–CdSe QDs structure was characterized with different spectroscopic techniques. The crystallinity and the phase formation of MPA–CdSe confirmed by the X-ray diffraction, which shows the dominance of cubic over the hexagonal phase (Fig. 2). The size of MPA–CdSe was determined using Debye–Scherrer [18] equation (1) by the FWHM of the characteristic peak (1 1 1) as follow:

$$L = \frac{K_S\, l}{b \cos q} \tag{1}$$

where L is the coherence length, β is the full width at half maximum of the peak, λ is the wavelength of X-ray radiation (1.5406 Å), *K*s is the Scherrer constant of the order of unity (0.95) and θ is the angle of diffraction for (111) plane. The average size was calculated as 3 nm taking into account that L = ¾ D, where D is the nanoparticles diameter, in case of small crystallites.

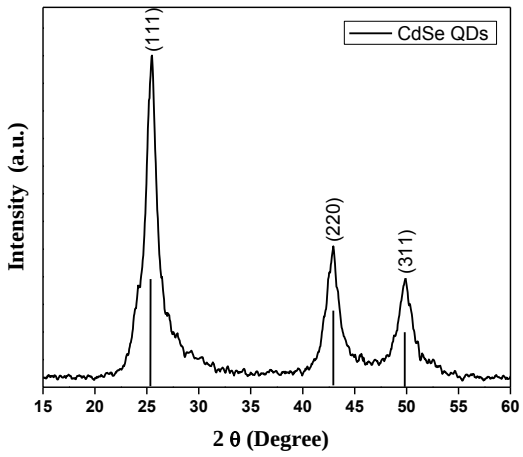

Fig. 2. XRD pattern of MPA capped CdSe QDs.

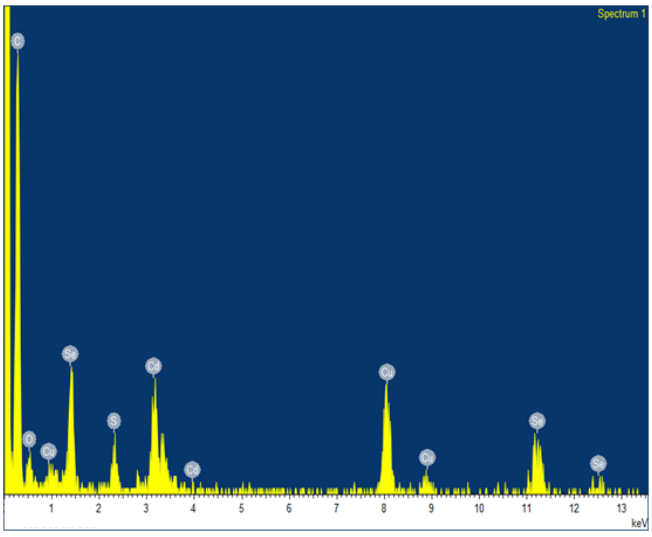

Fig. 3. The EDAX spectrum of CdSe QDs.

Energy-dispersive X-ray analysis (EDAX) spectrum of CdSe nanocrystalline powder was shown in Figure 3. The corresponding energy-dispersive X-ray spectrometry (EDAX) results indicated the presence of Cd, Se in these nanocrystalline as well as the S element. The Cd and Se were from CdSe and the S was attributed to the stabilizer of mercaptopropionic acid (MPA).

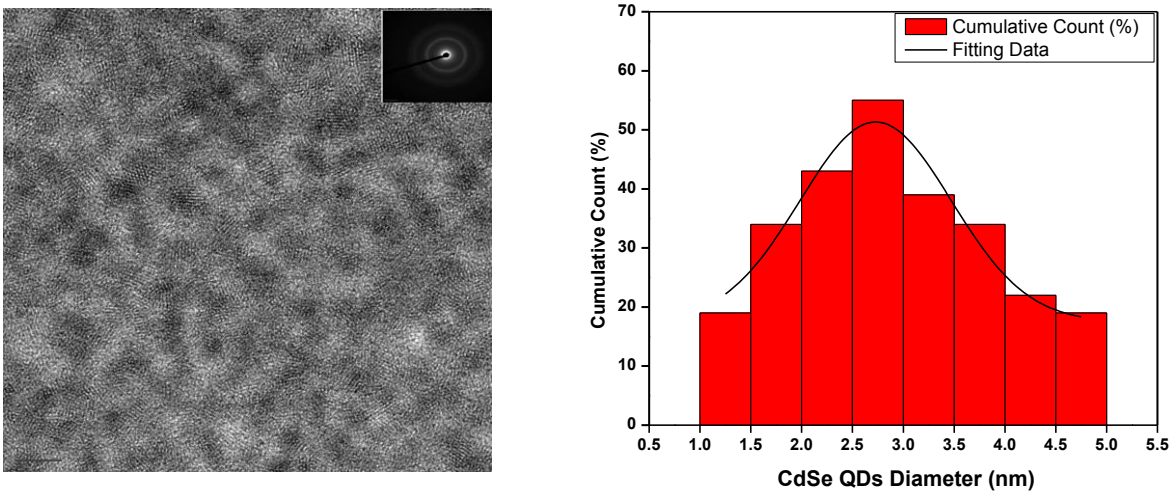

Fig. 4: TEM image and size dispersion histogram of the synthesized MPA-capped CdSe QDs (The scale bar equals 5 nm).

overMore, morphology and size distribution of CdSe nanocrystalline powder was analyzed using transmission electron microscope (TEM), (Figure 4). The average particle size calculated by log–normal fitting to the size distribution histogram, was calculated as 2.72 ± 0.025 nm. The matched particle size of MPA–CdSe nanocrystal obtained by both TEM with that of the calculated by X–ray confirm the crystalline nature of the nanocrystal.

The spectroscopic features of CdSe QDs capped with MPA were investigated by FT-IR. The FT-IR spectrum of the MPA capped CdSe nanocrystals were shown in Fig. 5. The broad peak at 3415 cm^{-1} corresponds to the combined effects of –OH stretching vibration. FT-IR spectra of pure capping agents show bands at 2565 cm^{-1} and 2665 cm^{-1} corresponding to S–H stretching [19]. The absence of these peaks in the prepared CdSe capped MPA indicates that thiol assisted capping took place around CdSe QDs with the concomitant loss of the S—H bond. In addition, the active mode peaks of CH_2 (2940 cm^{-1}) [20] in the capped layer are shifted to a lower frequency with respect to that of MPA for CdSe QDs (Fig. 5). The shift in CH_2 vibrations to smaller frequency indicates that the surfactant molecules in the adsorbed state are affected by the field of solid surface [20]. The vibration band of C-O observed at around 1717 cm^{-1} in the spectrum of pure capping agent [19] shifts to 1581 cm^{-1} for MPA-capped CdSe (Fig. 5), which indicates that thiol-capping chemically modifies the surface of CdSe QDs and the COOH was present in a state of COO^-, so that, the surface-modified CdSe QDs can be used as an analogous polyanionic compounds in the molecular deposition process.

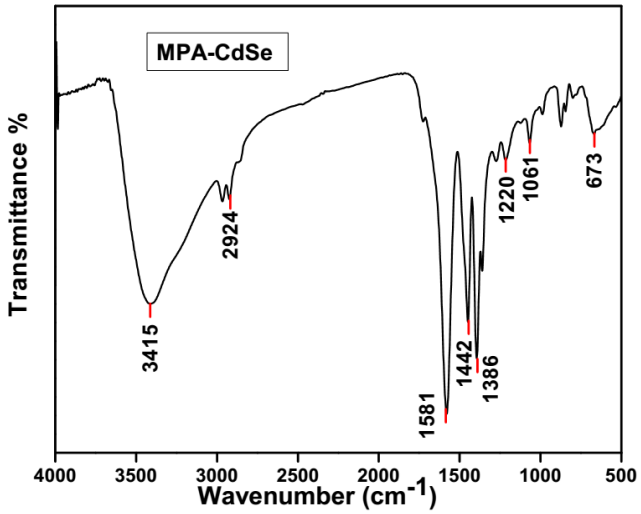

Fig. 5. FT-IR spectrum of CdSe nanocrystals capped with MPA.

3.2. Optical Properties of MPA–CdSe Nanocrystals

The UV-vis absorption spectra of MPA–CdSe are shown in Fig. 6. The absorption spectrum posses a broad band at 500 nm and narrow emission peak at 590 nm. The MPA–CdSe QDs particle size was calculated accordingly from the UV-vis absorption spectrum using equation (2) [21].

$$D = (1.6122\times10^{-9})\lambda^4-(2.6575\times10^{-6})\lambda^3+(1.6242\times10^{-3})\lambda^2-(0.4277)\lambda+(41.57) \quad (2)$$

Where, D (nm) is the size of a given MPA–CdSe QDs sample, and λ (nm) is the wavelength of the first excitonic absorption peak of the sample. The calculated average particle size is 2.35 nm, which agrees with TEM and XRD results. Then, the MPA–CdSe concentration were measured using Beer–Lambert law and the empirical formula ε = 10,043 $(D)^{2.12}$. The concentration of MPA–CdSe QDs was calculated as 2.78×10^{-7} M which, has been used in subsequent UV–vis and fluorescence measurements.

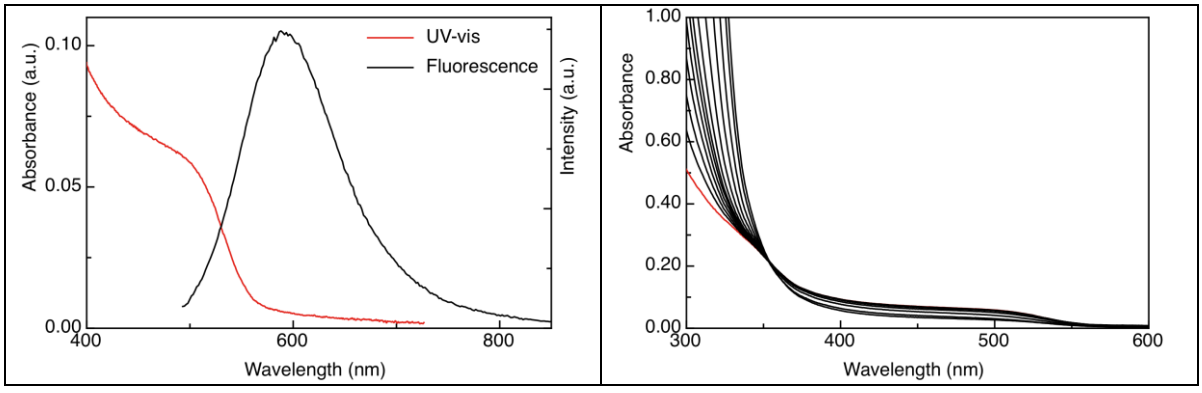

Fig. 6: a) Absorption spectra of MPA-capped CdSe QDs), red color, and emission spectra (2.78×10^{-7} M; λ_{exc} = 360 nm; λ_{emi} = 590 nm) black color, b) Absorption spectra of the prepared MPA-capped CdSe QDs (2.78×10^{-7} M), red color and successive concentration of acivicin.

To study the interaction between MPA–CdSe and acivicin, sodium acetate buffer at physiological pH value (7.7) were used. This was done to overcome the sensitivity of MPA–CdSe

for pH change. The sensitivity of MPA–CdSe pH change, higher fluorescence intensity at high pH and decreasing at low pH values with a red peak shift, probably due to increase in size and/or aggregation [19,22-25].

3.3. MPA–CdSe Interaction with Antibiotics

The MPA–CdSe QDs fluorescence spectra shows peak at 590 nm ($\lambda_{ex.}$ =390 nm, Fig 7). The excitation wavelength was selected where the interaction of MPA–CdSe nanocrystal and antibiotic posses minimum absorption change (isosbestic point, Figure 7). Upon addition of the successive concentration of the antibiotic (acivicin), the peak intensity at 590 nm was decreased. Stern-Volmer equation [26] (equation 4) was used to determine the quenching of QDs by antibiotic as shown below.

$$I_0/I = 1 + K_{SV}[Q] = 1 + k_q\tau_0[Q] \quad (4)$$

Where, I_0 and I are the emission intensities of QDs in absence and presence of the antibiotic respectively, K_{SV} is the Stern–Volmer quenching constant, k_q is the bimolecular quenching rate constant, τ_0 is the excited state lifetime of the QDs in absence of the quencher. [Q] is the concentration of the quencher.

The characteristic and sharp fluorescence peak at 590 nm of MPA–CdTe QDs (Figure 7), was used to monitor the interaction between the antibiotic and the QDs.

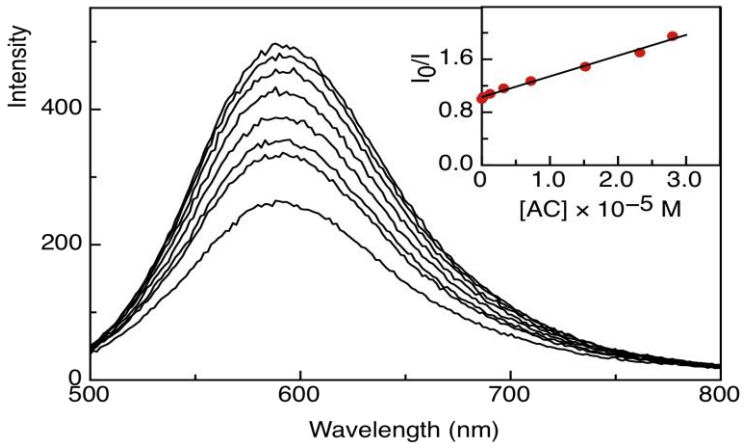

Fig. 7 Fluorescence quenching of MPA–CdSe QDs (2.78 × 10^{-7} M; λ_{exc} = 390 nm; λ_{emi} = 590 nm) in the presence of various concentrations of AC, [AC] = 0, 0.02, 0.07, 0.18, 0.40, 0.9, 1.9, and 3.2 × 10^{-5} M. Inset is the Stern–Volmer plot for the quenching of MPA–CdSe QDs by AC.

On applying Stern–Volmer equation, a linear relation (r =0.98) is obtained and K_{SV} = 0.26 × 10^2 LM^{-1} was obtained from the slope of the plot (Fig. 7, inset). Taking into account that the fluorescence lifetime (τ_0) of the bimolecular is 10^{-8} s, the bimolecular quenching constant calculated from the relation k_q is 1.3 × 10^9 M^{-1} s^{-1}. The value that is lower than the collision constant of bimolecular reactions, which suggests that AC quench the QDs by dynamic quenching mechanism. The interaction mechanism is shown in Fig. 7. The interaction between AC and the QDs occurs by dynamic quenching mechanism, which predicts that the possible interaction mainly proceeds by an electrostatic interaction between the electronegative surface of the QDs and the positive charge on AC (Fig.8)

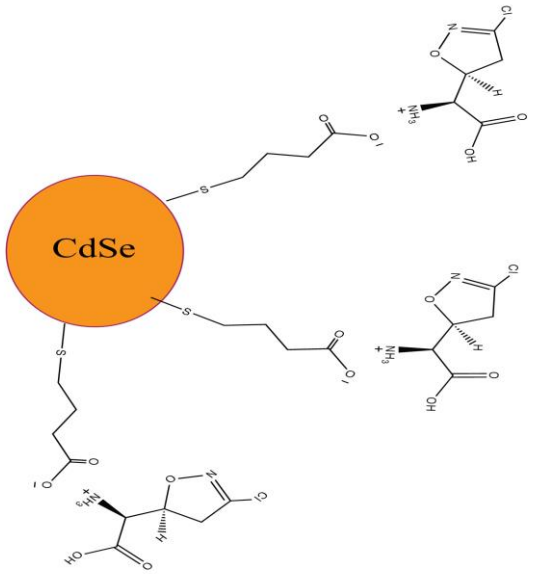

Fig.8. The structure of CdSe QDs–AC and the model of the hydrophobic force between CdSe QDs–AC.

Moreover, we investigated the fluorescence lifetime of the QDs in absence and presence of AC to further confirms that the quenching of MPA-CdSe by AC is dynamic rather than static quenching. Time-resolved fluorescence measurements of the QDs exhibit a mono-exponential lifetime decay with 8.20 ns average life time (Fig. 9). The addition of successive AC concentration quenches the lifetime to 6.25 ns (200 uM AC), which is a typical behavior for the dynamic quenching mechanism [27].

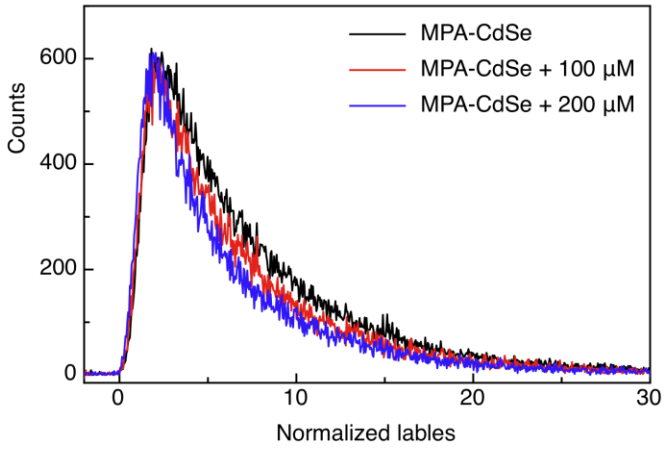

Fig. 9 Fluorescence decay kinetics of MPA-CdSe in 50 mM sodium acetate in absence and presence of different concentrations of the antibiotic (AC).

3.4. Conformational change of HAS induced by CdSe-AC complex

Effect of MPA-CdSe-AC complex on the secondary structure of HAS was recorded using Circular Dichroism (CD) spectra (Fig. 10). The far-UV CD spectra of HAS exhibits two negative bands in the UV region at 208 and 222 nm, which ascribed to the α-helical structure of HAS and the n $\rightarrow$ π* transfer for the peptides bonds in α-helical [28]. Upon addition of different concentrations of MPA-CdSe-AC complex, remarkable decrease in the band intensity at the two wavelengths was observed. The different types of the secondary structures contents was

investigated by analyzing the CD spectra with the algorithm SELCON3 [29,30]. The results show a decreasing tendency for the α-helices content and an increasing tendency of the β-strands, turn, and unordered structure contents were observed with the concentration of QDs-AC complex. In particular, the α-helices content decreases from 58% to 33% and the β-strands increases from 48.2% to 53.8%. Of note, such influence of the QDs-AC complex on the structure confirmation of HSA is higher than the antibiotic on the HAS structure. Quantitative analysis of the effect of the AC on the HAS structure confirmation showed that the decrease of α-helices content from 57.4% to 52% and an increase of the β-strands from 48% to 50%. The decrease of the α-helices and the increase of the β-strands contents indicated that the QDs-AC complex bounds more strongly with the main polypeptide chain of the HSA than the AC and destroy their hydrogen bond networks [31].

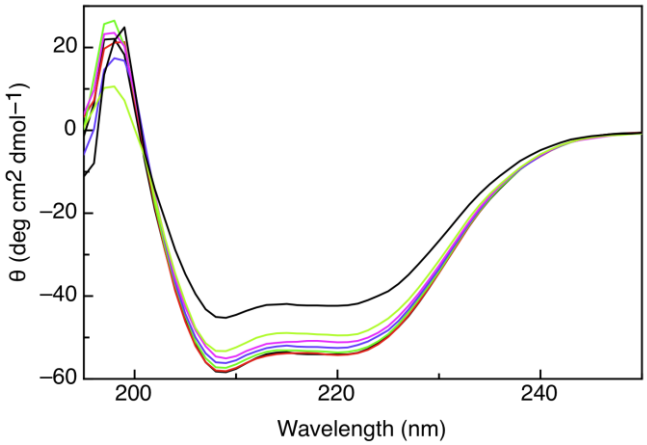

Fig. 10 The far-UV CD spectra of the QDs–HAS complex obtained in 50 mM Sodium acetate Buffer of pH 7.4 at room temperature. The concentration of HSA was 4 μM.

4. Conclusion

MPA–CdSe QDs were synthesized by facial and reliable chemical rout. The obtained QDs were investigated with both optical and spectroscopic techniques. Both methods confirm the 2.35 nm particle size for MPA–CdSe QDs. The as prepared MPA–CdSe QDs possess narrow emission peak peak at 590 nm that decrease in intensity with decreasing the pH value and increasing temperature. The long wavelength fluorescence peak was used to study the interaction between CdSe QDs acivicin (AC) that shows a dynamic quenching process. The interaction between AC and the QDs occurs by dynamic quenching mechanism, which predicts that the possible interaction mainly proceeds by an electrostatic interaction between the electronegative surface of the QDs and the positive charge on AC. Time-resolved fluorescence measurements of the bar QDs exhibit a mono-exponential life time decay with 8.20 ns average life time.

Acknowledgment

This work was funded by the Deanship of Scientific Research (DSR), King Abdulaziz University, Jeddah, under grant No. (363-005-D1433). The authors, therefore, acknowledge with thanks DSR technical and financial support.

Reference

[1] M. Zhang, X. Cao, H. Li, F. Guan, J. Guo, F. Shen, Y. Luo, C. Sun and L. Zhang, Food Chem., **135**, 1894 (2012).
[2] N. Kosaka, M. Mitsunaga, P.L. Choyke and H. Kobayashi, Contrast Media Mol. I., **8,** 96 (2013).
[3] Y. Zakharko, T. Serdiuk, T. Nychyporuk, A. Geloen, M. Lemiti and V. Lysenko, Plasmonics, **7**, 725 (2012) .
[4] A. Jaiswal, S.S. Ghsoh, A. Chattopadhyay, Langmuir **28**, 15687 (2012).
[5] M.J. Ruedas-Rama, J.D. Walters, A. Orte and E.A.H. Hall, Anal. chim. acta, **751**, 1 (2012).
[6] T.-T. Gan, Y.-J. Zhang, N.-J. Zhao, X. Xiao, G.-F. Yin, S.-H. Yu, H.-B. Wang, J.-B. Duan, C.-Y. Shi, W.-Q. Liu, Spectrochimica acta A, **99**, 62 (2012).
[7] Y. Yin, A.P. Alivisatos, Nature, **437**, 664 (2005).
[8] T.M. Samir, M.M.H. Mansour, S.C. Kazmierczak and H.M.E. Azzazy, Nanomedicine, **7**, 1755 (2012).
[9] T.C. King-Heiden, P.N. Wiecinski, A.N. Mangham, K.M. Metz, D. Nesbit, J.A. Pedersen, R.J. Hamers, W. Heideman and R.E. Peterson, Environ. Sci. Technol., **43**, 1605 (2009).
[10] T.S. Hauck, R.E. Anderson, H.C. Fischer, S. Newbigging and W.C.W. Chan, Small, **6**, 138 (2010).
[11] B. Dubertret, P. Skourides, D.J. Norris, V. Noireaux, A.H. Brivanlou, A. Libchaber, Science, **298**, 1759 (2002).
[12] E. Chang, N. Thekkek, W.W. Yu, V.L. Colvin and R. Drezek, Small, **2**, 1412 (2006).
[13] Ashley N. Brown, Kathryn Smith, Tova A. Samuels, Jiangrui Lu, Sherine O. Obare, Maria E. Scott, Applied and Environmental Microbiology (2012) 2768.
[14] Kalan L, Wright G. D, Expert Rev. Mol. Med. **13**, e5 (2011).
[15] Larissa Brentano Capeletti, Luciane França de Oliveira, Kaliandra de Almeida Gonçalves, Jessica Fernanda Affonso de Oliveira, Ângela Saito, Jörg Kobarg, João Henrique Zimnoch dos Santos, and Mateus Borba Cardoso, Langmuir **30**, 7456 (2014).
[16] Johannes Kreuzer, Nina C. Bach, Daniel Forler and Stephan A. Sieber, Chem. Sci., **6**, 237 (2015).
[17] Viet Ha Chu, Thi Ha Lien Nghiem, Tien Ha Le, Dinh Lam Vu, Hong Nhung Tran, Thi Kim Lien Vu, Adv. Nat. Sci.: Nanosci. Nanotechnol. **3**, 025017 (2012).
[18] Guinier A., X-Ray Diffraction: In Crystals, Imperfect Crystals, and Amorphous Bodies, W. H. Freeman & Company, San Francisco, USA, Chapter 2, 1963.
[19] H. S. El-Sheshtawy, M. S. Abd El Sadek, and I. S. Yahia, Nanosci. Nanotechnol. Lett. **6**, 18 (2014).
[20] M. S. Abd El-sadek, A. Y. Nooralden, S. Moorthy Babu, and P. K. Palanisamy, Opt. Commun. **284**, 2900(2011).
[21] W. William Yu, Lianhua Qu, Wenzhuo Guo, and Xiaogang Peng., Chem. Mater., **15**, 2854 (2003).
[22] Y. Yu, L. Xu, J. Chen, H. Gao, S. Wang, J. Fang and S. Xu, Colloids Surf. B, **95**, 247 (2012).
[23] D. Mutavdzic, J. Xu, G. Thakur, R. Triulzi, S. Kasas, M. Jeremic, R. Leblanc, K. Radotic, Analyst, **136**, 2391 (2011).
[24] A. Mandal and N. Tamai, J. Phys. Chem. C, 112 (2008) 8244.
[25] Y. Zhang, L. Mi, P.-N. Wang, J. Ma and J.-Y. Chen, J. of Lumin., **128,** 1948 (2008).
[26] J.R. Lakowicz, Principles of Fluorescence Spectroscopy, Plenum Press, New York, 2006.
[27] J.R. Lakowicz, Principles of Fluorescence Spectroscopy, Third ed., Springer, New York, 2006.
[28] L.Zhao, R.Liu, X.Zhao, B.Yang, C.Gao, X.Hao and Y.Wu, Sci. Total. Environ., **407**, 5019 (2009).
[29] L. Whitmore and B.A. Wallace, Nucleic Acids Res., **32**, W668 (2004).
[30] N. Sreerama, R.W. Woody, Anal. Biochem. , **209**, 32 (1993).
[31] F.L. Cui, J. Fan, J.P. Li, Z.D. Hu, Bioorg. Med. Chem., **12**, 151 (2004).